IEEE Access
Multidisciplinary | Rapid Review | Open Access Journal

Received March 5, 2017, accepted March 23, 2017, date of publication March 30, 2017, date of current version May 17, 2017.

Digital Object Identifier 10.1109/ACCESS.2017.2689773

Synchronous Flux Weakening Control With Flux Linkage Prediction for Doubly-Fed Wind Power Generation Systems

MENG WANG[1], YANYAN SHI[1], ZHENYANG ZHANG[1], MINGHUI SHEN[2], AND YAYING LU[1]
[1]School of Electronic and Electrical Engineering, Henan Normal University, Xinxiang 453007, China
[2]State Grid Xinxiang Power Company, Xinxiang 453000, China

Corresponding author: Y. Shi (yyshi113@hotmail.com)

This work was supported in part by the National Natural Science Foundation of China under Grant 61640303, in part by the Natural Science Foundation of Henan Province of China under Grant 162300410173, and in part by the Key Science and Technology Project of Henan Province of China under Grant 152102210084 and Grant 172102210354.

ABSTRACT Under grid-voltage dips, there exist dc and negative sequence components in the stator and rotor flux of doubly-fed induction generator (DFIG). As a result, higher transient overcurrent is generated in the rotor. To enhance the low-voltage ride-through (LVRT) ability of the DFIG, a synchronous flux weaken control strategy with flux linkage prediction is proposed to suppress the transient overcurrent. In the proposed control strategy, the deadbeat predictive control is used to realize rapid synchronization and weak interaction between the stator and rotor flux by flux linkage prediction under grid-voltage dips. A series of research is carried out on a typical 1.5-MW DFIG system, and comparisons are made with the LVRT control strategy based on proportional-resonant (PR) controller to validate the proposed control strategy. The results indicate that the proposed control strategy is effective in suppressing overcurrent in the stator and rotor and reducing oscillations in torque, which largely improves the performance of the DFIG during grid-voltage dips.

INDEX TERMS DFIG, flux linkage prediction, flux weakening control, deadbeat predictive control.

I. INTRODUCTION

In recent years, extensive research has been focused on wind power generation [1], [2]. Wind turbines based on doubly-fed induction generator (DFIG) is widely adopted in the wind market due to its variable speed constant frequency ability and excellent speed regulation performance [3]–[5]. For DFIG, the capacity of the power converter is only 30% of that of the generator, which reduces the cost of the system. However, the power converter with small capacity is not beneficial for the low-voltage ride-through (LVRT) control. This is a great challenge for the further development of DFIG during grid voltage dips.

DFIG is very sensitive to the grid disturbance especially to grid dips as the stator windings are directly connected to the grid. The control of DFIG is realized by PWM converter which is directly connected to the rotor. Due to the small capacity and weak control ability of the PWM converter, the suppression of the fault overcurrent is limited. Currently, a possible way to enhance the LVRT capability is the installation of a crowbar across the rotor terminals. With the release of energy through the bypass protection resistance, the rotor current is reduced and LVRT during grid dips is implemented [6], [7]. However, a large amount of reactive power is consumed from the grid as the DFIG behaves like a general induction generator, leading to further degradation of grid faults [8], [9]. Besides, the hardware cost is increased. During grid voltage drops, the mathematical model of the DFIG is established in positive and negative synchronous reference frame [10]. According to the difference of the control targets, positive and negative sequence decomposition of the variables is conducted and proportion integral (PI) regulators are employed in the control, which affects the dynamic performance and the response of the system. Excitation control of the DFIG is studied in [11]. By changing the proportional and integral coefficients of the PI regulator, the LVRT capability is improved within a certain range. However, it can be only applied to slight symmetrical three-phase grid voltage fault. In [12], the transient characteristics of the electromagnetic variables are analyzed for DFIG under symmetrical grid dips. The generators are controlled to counteract the undesirable effect of the transient DC component in the stator flux linkage, weakening the effect on the

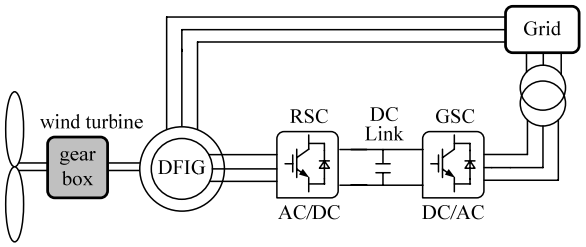

FIGURE 1. Block diagram of the DFIG-based system.

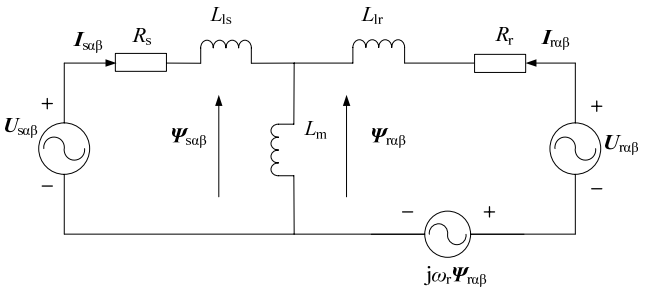

FIGURE 2. Equivalent circuit of DFIG in a two-phase stationary reference frame.

rotor and achieving LVRT. It has been demonstrated in [13] that feed-forward transient current control strategy is feasible to reduce the surge of the transient overcurrent on the DFIG. An improved direct power control approach is investigated for asymmetrical grid dips in [14]. The instantaneous active and reactive power of the stator is analyzed and two resonant controllers are utilized to achieve full control of output power and improve the robustness of the control system. Improved direct torque control and direct power control strategies are utilized in [15]. Under asymmetric dips, there is no need to extract the positive and negative sequence components. It has a simple structure and reduces the fluctuations in the power and electromagnetic torque. With predictive current control strategy, the dynamic response of the control system can be improved [16]. The controller has a fast response to the fault and the fault current can be suppressed quickly. Sliding mode control is used for DFIG in [17] and [18], which is effective in reducing oscillations of electromagnetic torque and reactive power.

In this work, a synchronous flux weakening control strategy with flux linkage prediction is proposed for DFIG. It considers the deadbeat predictive control strategy combined with a weakening flux control of the DFIG. In normal operation, a proportional-resonant (PR) control strategy based on two-phase stationary reference frame is applied to simplify coordinates transformation. During grid voltage drops, the control system is switched and the proposed control strategy is utilized. Firstly, the transient variation of the stator and rotor flux is investigated during grid faults. Then, to obtain the optimal referenced rotor flux, the relationship between the stator flux and rotor flux is deduced in two-phase stationary reference frame. At the moment of fault, with the fast prediction and quick response of the deadbeat controllers, the stator flux can be tracked by the rotor flux rapidly, which eliminates the impact of the stator flux on the rotor flux and weakens the fault current shock of the stator and the rotor. More stable electromagnetic torque is realized and the LVRT capability of DFIG is improved.

II. DFIG MODEL

The block diagram of the DFIG is illustrated in Fig. 1. The stator of the DFIG is directly connected to the grid while the rotor is excited by the double PWM back-to-back converters to ensure bi-directional energy flow.

As can be seen from Fig. 1, the double PWM back-to-back converters consist of rotor side converter(RSC) and grid side converter (GSC). The RSC is connected to the rotor to regulate the active and reactive power at the stator side while the GSC is connected to the grid by transformer to achieve power feedback to the grid and to ensure unity power factor.

Fig. 2 is the equivalent circuit of the DFIG in a two-phase stationary reference frame. The mathematical equations of the stator and rotor voltage and flux for a DFIG in the two-phase stationary reference frame can be described as

$$\begin{cases} \boldsymbol{U}_{s\alpha\beta} = R_s\boldsymbol{I}_{s\alpha\beta} + \mathrm{p}\boldsymbol{\Psi}_{s\alpha\beta}, \\ \boldsymbol{U}_{r\alpha\beta} = R_r\boldsymbol{I}_{r\alpha\beta} + \mathrm{p}\boldsymbol{\Psi}_{r\alpha\beta} - j\omega_r\boldsymbol{\Psi}_{r\alpha\beta} \end{cases} \tag{1}$$

$$\begin{cases} \boldsymbol{\Psi}_{s\alpha\beta} = L_\mathrm{s}\boldsymbol{I}_{s\alpha\beta} + L_\mathrm{m}\boldsymbol{I}_{r\alpha\beta} \\ \boldsymbol{\Psi}_{r\alpha\beta} = L_\mathrm{m}\boldsymbol{I}_{s\alpha\beta} + L_\mathrm{r}\boldsymbol{I}_{r\alpha\beta} \end{cases} \tag{2}$$

where $\boldsymbol{U}_{s\alpha\beta}$ and $\boldsymbol{U}_{r\alpha\beta}$ are the stator and rotor voltage, R_s and R_r are the stator and rotor resistance, $\boldsymbol{I}_{s\alpha\beta}$ and $\boldsymbol{I}_{r\alpha\beta}$ are the stator and rotor current, $\Psi_{s\alpha\beta}$ and $\Psi_{r\alpha\beta}$ are the stator and rotor flux, L_s, L_r and L_m, are the self-inductance of the stator and rotor and the mutual inductance, $L_\mathrm{s} = L_\mathrm{ls}+L_\mathrm{m}$, $L_\mathrm{r} = L_\mathrm{lr}+L_\mathrm{m}$, L_ls and L_lr are the stator leakage inductance and rotor leakage inductance, ω_r is the angular speed of the rotor and p is the differential operator.

The instantaneous active and reactive power output from the stator to the grid can be expressed as

$$\begin{cases} P_s = -1.5\left(u_{s\alpha}i_{s\alpha} + u_{s\beta}i_{s\beta}\right) \\ Q_s = -1.5\left(u_{s\beta}i_{s\alpha} - u_{s\alpha}i_{s\beta}\right) \end{cases} \tag{3}$$

where P_s and Q_s are stator active and reactive power, $u_{s\alpha}$ and $u_{s\beta}$ are α-axis and β-axis components of the stator voltage in the $\alpha\beta$ reference frame, $i_{s\alpha}$ and $i_{s\beta}$ are α-axis and β-axis components of the stator current.

The electromagnetic torque of the DFIG can be described as

$$T_e = n_pL_m\left(i_{s\beta}\Psi_{s\alpha} - i_{s\alpha}\Psi_{s\beta}\right) \tag{4}$$

where T_e stands for the electromagnetic torque, n_p is the number of pole pairs, $\Psi_{s\alpha}$ and $\Psi_{s\beta}$ are α-axis and β-axis components of the stator flux in the $\alpha\beta$ reference frame, respectively.

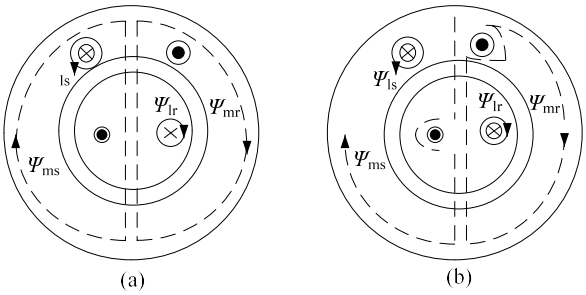

FIGURE 3. Magnetic circuit of stator and rotor.

Based on Eq. (1) and Eq. (2), the rotor voltage of the DFIG can be further expressed as

$$\begin{aligned} \boldsymbol{U}_{r\alpha\beta} &= (R_r - j\omega_r \sigma L_r)\boldsymbol{I}_{r\alpha\beta} + \sigma L_r p \boldsymbol{I}_{r\alpha\beta} \\ &\quad + L_m \left(\boldsymbol{U}_{s\alpha\beta} - R_s \boldsymbol{I}_{s\alpha\beta} - j\omega_r \boldsymbol{\Psi}_{s\alpha\beta}\right)/L_s \end{aligned} \tag{5}$$

where σ is the leakage coefficient and $\sigma = 1 - L_{\mathrm{m}}^2/(L_{\mathrm{s}}L_{\mathrm{r}})$.

Under normal operation, the α-axis and the β-axis components of the rotor current is regulated by the PR controller in the two-phase stationary reference frame as given in [19] and [20]. According to the PR control strategy, the rotor voltage can be designed as

$$\begin{aligned} \boldsymbol{U}^*_{r\alpha\beta} &= \sigma L_r \boldsymbol{U}^{'}_{r\alpha\beta} + (R_r - j\omega_r \sigma L_r)\boldsymbol{I}_{r\alpha\beta} \\ &\quad + L_m \left(\boldsymbol{U}_{s\alpha\beta} - R_s \boldsymbol{I}_{s\alpha\beta} - j\omega_r \boldsymbol{\Psi}_{s\alpha\beta}\right)/L_s \end{aligned} \tag{6}$$

where

$$\begin{aligned} \boldsymbol{U}^{'}_{r\alpha\beta} &= C_{PR}(s)\left(\boldsymbol{I}^*_{r\alpha\beta} - \boldsymbol{I}_{r\alpha\beta}\right) \\ &= \left[k_{ip} + \omega_{ic}k_{ir}s/\left(s^2 + 2\omega_{ic}s + \omega_e^2\right)\right]\left(\boldsymbol{I}^*_{r\alpha\beta} - \boldsymbol{I}_{r\alpha\beta}\right) \end{aligned} \tag{7}$$

and where $\boldsymbol{U}^*_{\mathrm{r}\alpha\beta}$ is voltage reference of the RSC, k_{ip}, k_{ir} and ω_{ic} are proportion, resonant and attenuation coefficient respectively, $C_{\mathrm{PR}}(s)$ stands for the PR controller, ω_{e} is the angular frequency of the grid voltage, $\boldsymbol{I}^*_{\mathrm{r}\alpha\beta}$ is rotor current reference.

III. SYNCHRONOUS FLUX WEAKENING CONTROL STRATEGY WITH FLUX LINKAGE PREDICTION

A. CHARACTERISTIC ANALYSIS OF DFIG UNDER GRID VOLTAGE DIPS

Fig. 3 shows the magnetic circuit of the stator and rotor for the DFIG under the normal operation and the grid dips respectively.

It can be seen from Fig. 3 that the magnetic circuit changes in case of grid dips. In normal operation, the armature magnetic field Ψ_{ms} and the magnetic field excitation Ψ_{mr} come across the air gap through the main magnetic circuit and the stator is linked with rotor windings. Under grid dips, Ψ_{ms} comes across the rotor magnetic leakage circuits without crossing the rotor windings and Ψ_{mr} comes across the stator magnetic leakage circuits without crossing the stator windings. The self-inductance of the stator and rotor is dependent on the magnetic circuit in the stator and rotor windings, which further affects the stator and rotor flux. However, transient change in the stator and rotor flux will result in higher transient current.

In the condition of grid voltage dips, the stator voltage sages which in turn causes transient DC and negative sequence components appear in the stator flux. A larger fault current occurs in the rotor. The stator flux in the two-phase stationary reference frame can be described as

$$\begin{aligned} \boldsymbol{\Psi}_{s\alpha\beta}(t) &= \boldsymbol{\Psi}_{s\alpha\beta+}(t) + \boldsymbol{\Psi}_{s\alpha\beta\ \mathrm{DC}}(t) + \boldsymbol{\Psi}_{s\alpha\beta-}(t) \\ &= \left|\boldsymbol{\Psi}_{s\alpha\beta+}\right| e^{j(\omega_e t+\varphi_+)} + \left|\boldsymbol{\Psi}_{s\alpha\beta\ \mathrm{DC}}\right| e^{-t/\tau_s} \\ &\quad + \left|\boldsymbol{\Psi}_{s\alpha\beta-}\right| e^{-j(\omega_e t+\varphi_-)} \end{aligned} \tag{8}$$

where the subscripts s, $\alpha\beta$, +, - and DC represent the stator flux, stationary $\alpha\beta$ axis, positive sequence component, negative sequence component and DC component, respectively; τ_{s} stands for the attenuation time constant of the DC component; φ_+ and φ_- stand for the initial phase angles of the positive and negative sequence component of stator flux.

B. THE PROPOSED CONTROL STRATEGY

As strong coupling exists between the stator and the rotor, the DC and negative sequence components in the stator flux induce overcurrent in the rotor. Therefore, the interaction between the stator and rotor flux must be reduced during the grid dips. In this work, the rotor flux is controlled to be synchronized with the stator flux and the interaction between the stator and rotor flux is weakened. According to Eq. (2), the stator current can be calculated as

$$\boldsymbol{I}_{s\alpha\beta} = \frac{L_{\mathrm{r}}\boldsymbol{\Psi}_{s\alpha\beta} - L_{\mathrm{m}}\boldsymbol{\Psi}_{r\alpha\beta}}{L_{\mathrm{r}}L_{\mathrm{s}} - L_{\mathrm{m}}^2} \tag{9}$$

Assuming $L_{\mathrm{s}}/L_{\mathrm{m}} \approx 1$, the rotor current can be given as

$$\boldsymbol{I}_{r\alpha\beta} = \frac{L_m}{L_s L_r - L_m^2}\left(\boldsymbol{\Psi}_{r\alpha\beta} - \boldsymbol{\Psi}_{s\alpha\beta}\right) \approx \frac{\boldsymbol{\Psi}_{r\alpha\beta} - \boldsymbol{\Psi}_{s\alpha\beta}}{L_{ls} + L_{lr}} \tag{10}$$

From Eq. (9) and Eq. (10), it can be observed that the variation of the stator and rotor flux is related to the stator and rotor current. Thus, the stator and rotor overcurrent can be effectively suppressed when the stator and the rotor flux change synchronously at the instant of the grid dips. The relationship between the stator and rotor flux can be established as

$$\boldsymbol{\Psi}_{r\alpha\beta} = M\boldsymbol{\Psi}_{s\alpha\beta} \tag{11}$$

where M is a propotional variation.

The rotor current can be obtained by substituting Eq. (11) into Eq. (10) as

$$\boldsymbol{I}_{r\alpha\beta} \approx \frac{M\boldsymbol{\Psi}_{s\alpha\beta} - \boldsymbol{\Psi}_{s\alpha\beta}}{L_{ls} + L_{lr}} \tag{12}$$

Substitute Eq. (11) into Eq. (9), M can be computed as

$$M = \frac{L_{\mathrm{r}}}{L_{\mathrm{m}}} - \frac{I_{s\alpha\beta}(L_{\mathrm{r}}L_{\mathrm{s}} - L_{\mathrm{m}}^2)}{L_{\mathrm{m}}\boldsymbol{\Psi}_{s\alpha\beta}} \tag{13}$$

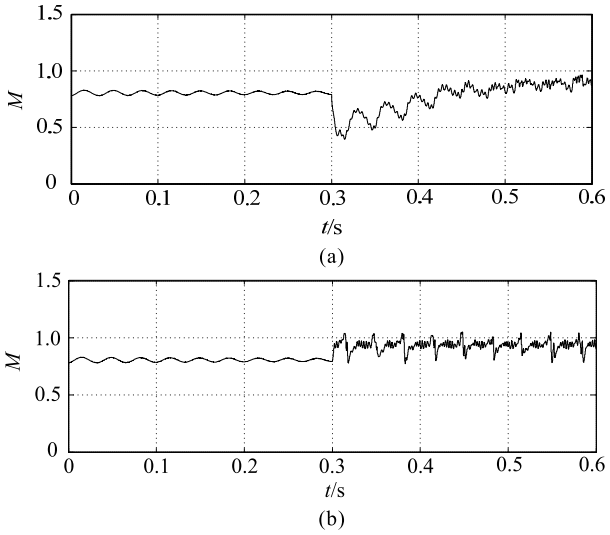

FIGURE 4. The variation of M under the symmetrical and asymmetrical dips. (a) symmetrical dips. (b) asymmetrical dips.

Based on Eq.(13), the variation of M is shown in Fig. 4 when symmetrical and asymmetrical dips occur at $t = 0.3$ s.

As can be seen from Fig. 4(a), when the symmetrical grid voltage dips occurs, M has a larger oscillation at first and gradually returns to the normal state. As can be seen from Fig. 4(b), when the asymmetrical dips occurs, M has a smaller oscillation while M keeps in a fluctuation state.

In order to eliminate the interaction between the stator and the rotor flux, the rotor flux is controlled to be synchronized with the stator flux by Eq. (11). The rotor voltage in Eq. (1) can be described in the two-phase stationary reference frame as

$$\begin{cases} u_{r\alpha} = R_r i_{r\alpha} + p\Psi_{r\alpha} + \omega_r \Psi_{r\beta} \\ u_{r\beta} = R_r i_{r\beta} + p\Psi_{r\beta} - \omega_r \Psi_{r\alpha} \end{cases} \tag{14}$$

Eq. (14) can be discretized to obtain the output voltage in the deadbeat predictive control as

$$\begin{cases} u_{r\alpha}(k) = R_{\mathrm{r}} i_{r\alpha}(k) + \omega_r(k)\Psi_{r\beta}(k) \\ \qquad + \dfrac{1}{T_s}\left[\Psi_{r\alpha}(k+1) - \Psi_{r\alpha}(k)\right] \\ u_{r\beta}(k) = R_{\mathrm{r}} i_{r\beta}(k) - \omega_r(k)\Psi_{r\alpha}(k) \\ \qquad + \dfrac{1}{T_s}\left[\Psi_{r\beta}(k+1) - \Psi_{r\beta}(k)\right] \end{cases} \tag{15}$$

where T_{s} is the sampling period, k+1 and$k$are the sampling time.

At the kth sampling time, the variables in Eq. (15) are sampled, where the rotor flux at the (k+1)th sampling time is replaced by the referenced value. The rotor flux reference is as follows

$$\boldsymbol{\Psi}^*_{r\alpha\beta} = M\boldsymbol{\Psi}_{s\alpha\beta} \tag{16}$$

where superscript $*$ represents the referenced value.

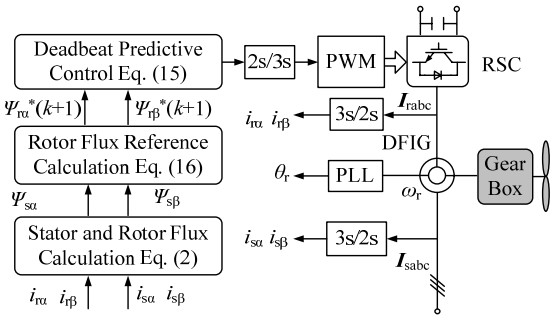

FIGURE 5. Block diagram of the proposed control strategy.

Based on the deadbeat predictive control of the rotor flux, the actual rotor flux is able to track the referenced value and synchronous flux weakening control is realized.

Fig. 5 is the block diagram of the proposed synchronous flux weakening control with flux linkage prediction for DFIG. The stator current I_{sabc} and the rotor current I_{rabc} are firstly detected. After coordinate transformation, the stator current $i_{\mathrm{s}\alpha}$, $i_{\mathrm{s}\beta}$ and the rotor current $i_{\mathrm{r}\alpha}$, $i_{\mathrm{r}\beta}$ are obtained in the two-phase stationary reference frame. Based on the self-inductance of the stator and the rotor and the mutual inductance, the stator flux $\Psi_{\mathrm{s}\alpha}$, $\Psi_{\mathrm{s}\beta}$ and the rotor flux $\Psi_{\mathrm{r}\alpha}$, $\Psi_{\mathrm{r}\beta}$ are calculated, which will be controlled by the synchronous flux weakening control. In other words, the rotor flux reference $\Psi^*_{\mathrm{r}\alpha}$ and $\Psi^*_{\mathrm{r}\beta}$ is calculated and referred as the input of the deadbeat predictive control. In this way, the rotor voltage in two-phase stationary reference frame can be obtained and three-phase rotor voltage is acquired through coordinate transformation. Finally, the control signal of the RSC is generated through PWM modulation.

C. STABILITY ANALYSIS

Under grid voltage dips, The higher transient overcurrent in the stator and rotor causes magnetic saturation and inductance mismatch, leading to instability of the deadbeat predictive control [21]. In Eq. (15), ω_{r} is much smaller than $1/T_{\mathrm{s}}$ where $T_{\mathrm{s}} = 5\mathrm{e}\text{-}5$. Therefore, the rotor actual voltage on α-axis can be simplified as

$$u_{r\alpha}(k) = R_{\mathrm{r}} i_{r\alpha}(k) + \frac{1}{T_s}\left[\Psi_{r\alpha}(k+1) - \Psi_{r\alpha}(k)\right] \tag{17}$$

With the proposed control strategy, the deadbeat predictive controller could be realized by

$$u_{r\alpha}(k) = R_{\mathrm{r}} i_{r\alpha}(k) + \frac{1}{T_s}\left[\Psi^*_{r\alpha}(k+1) - \Psi_{r\alpha}(k)\right] \tag{18}$$

The rotor flux in Eq. (2) can be described in two-phase stationary reference frame as

$$\begin{cases} \Psi_{r\alpha} = L_m i_{s\alpha} + L_r i_{r\alpha} \\ \Psi_{r\beta} = L_m i_{s\beta} + L_r i_{r\beta} \end{cases} \tag{19}$$

where $\Psi_{\mathrm{s}\alpha}$ and $\Psi_{\mathrm{s}\beta}$ are the α-axis and β-axis components of the stator flux, $i_{\mathrm{r}\alpha}$ and $i_{\mathrm{r}\beta}$ are the α-axis and β-axis components of the rotor current.

It can be seen from the Eq. (19) that inductance mismatch leads to rotor flux mismatch. In addition, the rotor resistance also varies with the temperature of the generator.

In order to study the impact of the parameters on the system stability, weighting factors a and b are added to the α-axis component of the rotor flux and to the rotor resistance, respectively. The rotor flux and the resistance can then be obtained as

$$\begin{cases} \Psi_{r\alpha}^{m} = a \times \Psi_{r\alpha} \\ R_r^m = b \times R_r \end{cases} \tag{20}$$

where the superscript m denotes the variable in the deadbeat predictive control.

According to characteristics of the inductance and the resistance of the generator, the flux and the resistance changes to a certain extent. In the deadbeat predictive control, the control performance is closely related to the difference between the rotor flux at the $(k+1)$th sampling time and that at the kth sampling time. Therefore, a weighting factor c is added and the rotor voltage on α-axis can be described as

$$u_{r\alpha}(k) = R_r^m i_{r\alpha}(k) + \frac{c}{T_s}\left[\Psi_{r\alpha}^{m}(k+1) - \Psi_{r\alpha}^{m}(k)\right] \tag{21}$$

Substituting Eq. (21) into Eq. (17), it can be obtained as

$$\begin{aligned} &\Psi_{r\alpha}(k+1) - (1 - a \times c)\,\Psi_{r\alpha}(k) \\ &\quad = a \times c \times \Psi_{r\alpha}^{m}(k+1) - (1-b) \times R_r \times i_{r\alpha}(k) \times T_s \end{aligned} \tag{22}$$

In Eq. (22), the second term at the right of the equation is very small and can be neglected. The discrete transfer function of the Eq. (21) is given as

$$\frac{\Psi_{r\alpha}(z)}{\Psi_{r\alpha}^{m}(z)} = \frac{a \times c \times z}{z - (1 - a \times c)} \tag{23}$$

According to Eq. (23), Eq. (18) is stable only when a and c satisfy

$$0 < a \times c < 2 \tag{24}$$

In conclusion, the rotor flux is within a certain range of error and a stable deadbeat predictive control system is attained.

Fig. 6 shows the relationship between characteristic roots Q_z of Eq. (23) and the weighting factors a and c. When the weight factors change, the scope of the characteristic root is analyzed to determine the stability of the system. The results show that the system is stable. When the weight factors a and c change, the characteristic roots Q_z are in the range of -1 to 1.

IV. RESULTS AND DISCUSSIONS

To validate the proposed control strategy, the performance of the DFIG with a 1.5-MW is investigated under grid voltage dips. Besides, comparisons are carried out between the PR control strategy for LVRT used in [19] and the proposed method. The main parameters of the DFIG system are given in Table 1.

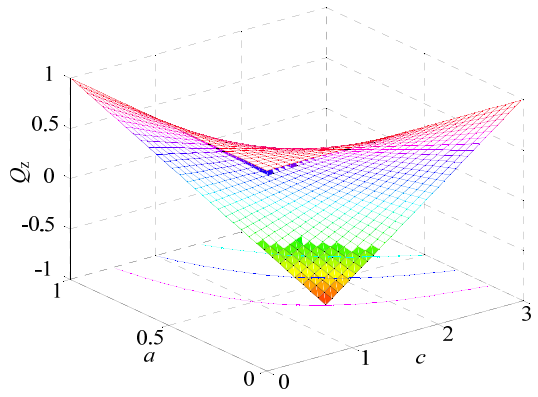

FIGURE 6. Stability analysis.

TABLE 1. The main parameters of the DFIG.

Parameters	Value
Rated generator power	1.5MW
Rated generator voltage	575V
Frequency	60Hz
Stator resistance	0.0014Ω
Stator leakage inductance	8.998×10^{-5}H
Rotor resistance	$9.9187\times10^{-4}\Omega$
Rotor leakage inductance	8.2088×10^{-5}H
Magnetizing inductance	1.526×10^{-3}H
Pole pairs	3

When a 80% symmetrical dips occurs at the instant of $t = 0.3$ s, Fig. 7 shows the performance of the DFIG operated with the PR control strategy and the proposed control strategy respectively.

In Fig. 7(b), the electromagnetic torque fluctuates in the vicinity of zero and the impact on mechanical system is reduced, which enhances the LVRT ability of the DFIG under the grid dips. The stator and the rotor currents are controlled to be within their maximum allowed. Compared with Fig. 7(a), it can be observed that the proposed control strategy is more effective than the PR method when applied to eliminate the stator and rotor overcurrents and reduce oscillations of electromagnetic torque. Both of the two control strategies have an increase in rotor speed.

When a 60% single-phase dips occurs at the instant of $t = 0.3$ s, Fig. 8 shows the performance of DFIG operated with the PR control strategy and with the proposed control strategy respectively.

Comparing Fig. 8(a) and Fig. 8(b), it can be seen that the fluctuation of the electromagnetic torque is smaller when using the proposed control strategy which decreases the mechanical stress on the turbine system. The rotor fault current is effectively suppressed due to the weak interaction between the stator and rotor flux. Besides, the stator active power fluctuates around zero and its impact on the grid is reduced.

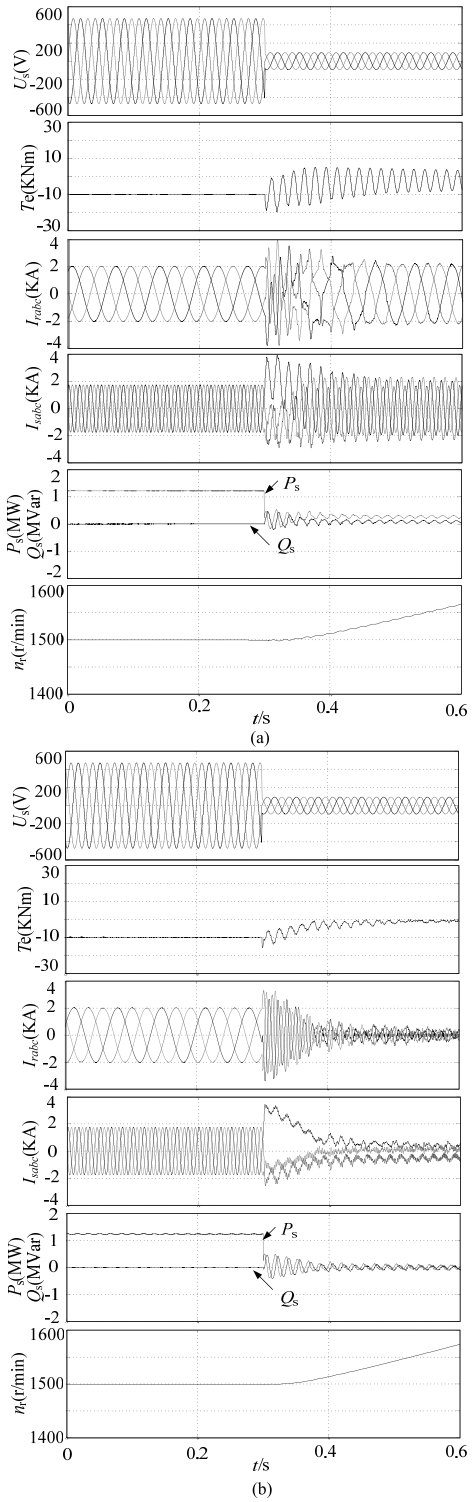

FIGURE 7. Operating results for a 80% symmetrical dips. (a) PR control strategy. (b) proposed control strategy.

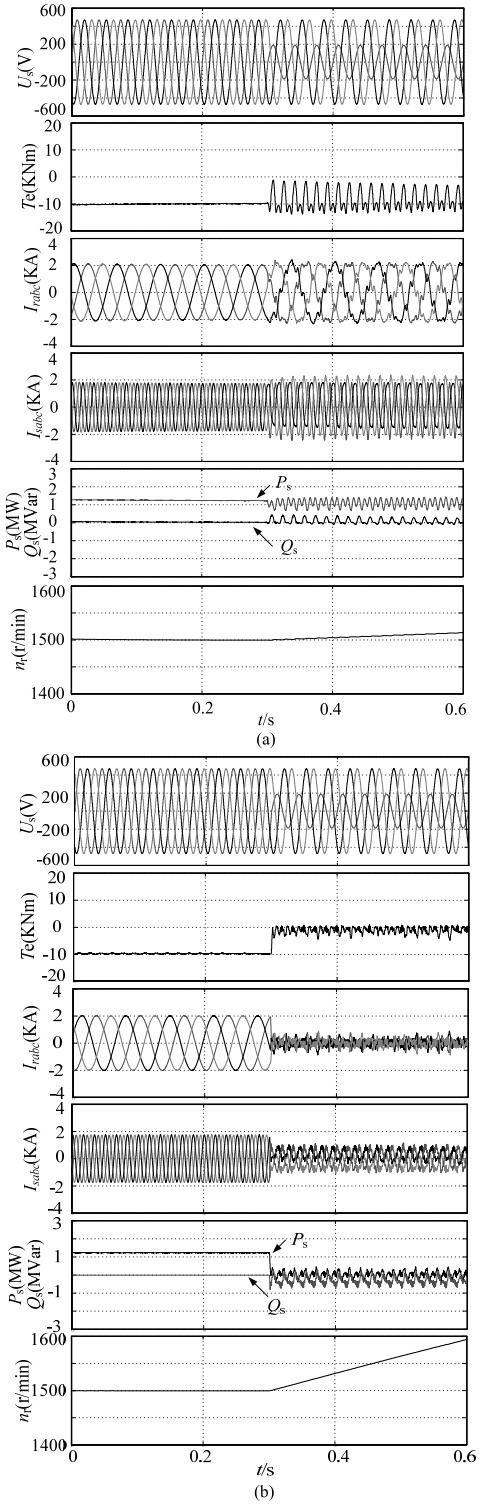

FIGURE 8. Operating results for a 60% single-phase dips. (a) PR control strategy. (b) proposed control strategy.

In order to verify the effectiveness of the proposed control strategy, Fig. 9 shows the dynamic responses of the DFIG system with the PR control strategy and with the proposed control strategy during multiple grid dips respectively. A 60% single-phase dips occurs at the instant of $t = 0.2$ s and a 80% symmetrical dips occurs at the instant of $t = 0.4$ s.

In Fig. 9(a), the electromagnetic torque has a large fluctuation when asymmetrical dips changes to symmetrical dips. Besides, the stator and rotor fault currents are further increased which leads to the deteriation of the RSC. The fluctuations of the stator active/reactive power are still obvious. However, in Fig, 9(b), the the electromagnetic torque

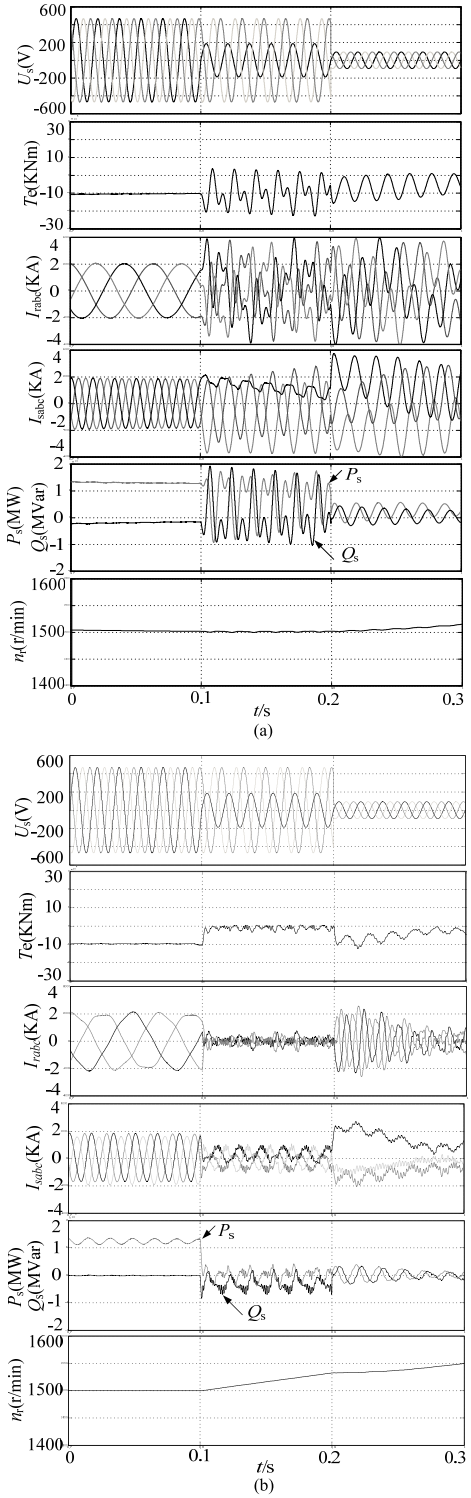

FIGURE 9. Operating results for multiple dips. (a) PR control strategy. (b) proposed control strategy.

has a smaller fluctuation when asymmetrical dips changes to symmetrical dips. The stator and rotor fault currents are controlled within maximum value of the RSC rating so the DFIG can ride through faults using the proposed control scheme. Furthermore, the stator active/reactive power becomes smaller and smaller which ensure the performance of the grid.

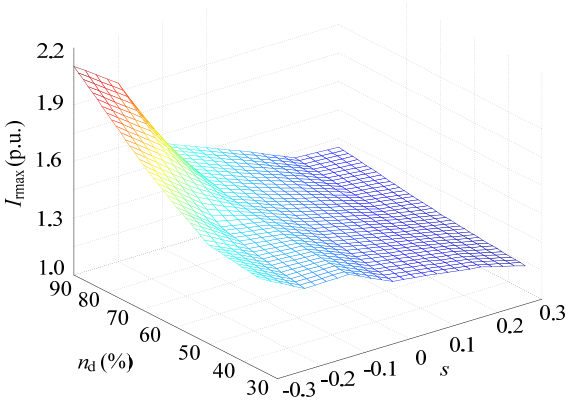

FIGURE 10. The maximum rotor dips current under different operating conditions.

Fig. 10 shows the maximum rotor dips currents under the condition of different grid voltage dips. n_d is the degree of symmetrical three-phase grid voltage dips, s is slip ratio of the DFIG and I_{rmax} is the maximum value of the rotor current.

As can be seen from Fig. 10, for the same slip ratio, when the symmetrical dips vary from 30% to 80%, the rotor current is controlled within the twice of the maximum current. Meantime, for the same drops, when the DFIG is operated at different slip ratios, the rotor current is controlled to be within the twice of the maximum current. Therefore, the proposed control strategy has improved LVRT ability.

V. CONCLUSION

In this study, a synchronous flux weakening control with flux linkage prediction is proposed for the doubly-fed WPGS. In the conditions of the symmetric and asymmetric dips, the deadbeat predictive control of the rotor flux is applied in order to realize synchronous flux weakening control of the stator and the rotor flux quickly. It suppresses the overcurrent caused by the interaction between the stator and the rotor, improving the stability margin and LVRT capability under the grid dips. The results show that the proposed control strategy has several advantages: 1) it is simple in the control structure and is easy to implement; 2) when a 80% symmetrical dips or a 60% single-phase dips occurs, moreover, including multiple dips, the stator and rotor currents can be controlled to be within the twice of the maximum current, weakening the impact on the transient overcurrent of the wind power system; 3) It is effective in eliminating the impact of the stator flux on the rotor flux, with a smaller fluctuation in the electromagnetic torque and reducing the mechanical shock of the grid dips on the generator.

REFERENCES

[1] Y. Li, Z. Xu, and K. Meng, "Optimal power sharing control of wind turbines," *IEEE Trans. Power Syst.*, vol. 32, no. 1, pp. 824–825, Jan. 2017.
[2] N. K. S. Naidu and B. Singh, "Grid-interfaced DFIG-based variable speed wind energy conversion system with power smoothening," *IEEE Trans. Sustain. Energy*, vol. 8, no. 1, pp. 51–58, Jan. 2017.
[3] Y. Ju, F. Ge, W. Wu, Y. Lin, and J. Wang, "Three-phase steady-state model of doubly fed induction generator considering various rotor speeds," *IEEE Access*, vol. 4, pp. 9479–9488, 2016.

[4] Y. Song, X. Wang, and F. Blaabjerg, "High-frequency resonance damping of DFIG-based wind power system under weak network," *IEEE Trans. Power Electron.*, vol. 32, no. 3, pp. 1927–1940, Mar. 2017.
[5] P. Cheng, H. Nian, C. Wu, and Z. Q. Zhu, "Direct stator current vector control strategy of DFIG without phase-locked loop during network unbalance," *IEEE Trans. Power Electron.*, vol. 32, no. 1, pp. 284–297, Jan. 2017.
[6] Z.-C. Zou, X.-Y. Xiao, Y.-F. Liu, Y. Zhang, and Y.-H. Wang, "Integrated protection of DFIG-based wind turbine with a resistive-type SFCL under symmetrical and asymmetrical faults," *IEEE Trans. Appl. Supercond.*, vol. 26, no. 7, Oct. 2016, Art. no. 5603005.
[7] K. E. Okedu, "Enhancing DFIG wind turbine during three-phase fault using parallel interleaved converters and dynamic resistor," *IET Renew. Power Generat.*, vol. 10, no. 8, pp. 1211–1219, Sep. 2016.
[8] W. Chen, D. Xu, N. Zhu, M. Chen, and F. Blaabjerg, "Control of doubly-fed induction generator to ride-through recurring grid faults," *IEEE Trans. Power Electron.*, vol. 31, no. 7, pp. 4831–4846, Jul. 2016.
[9] L.-J. Cai and I. Erlich, "Doubly fed induction generator controller design for the stable operation in weak grids," *IEEE Trans. Sustain. Energy*, vol. 6, no. 3, pp. 1078–1084, Jul. 2015.
[10] J. Li and K. Corzine, "Harmonic compensation for variable speed DFIG wind turbines using multiple reference frame theory," in *Proc. IEEE Appl. Power Electron. Conf. Expo.*, Mar. 2015, pp. 2974–2979.
[11] L. Holdsworth, X. G. Wu, J. B. Ekanayake, and N. Jenkins, "Comparison of fixed speed and doubly-fed induction wind turbines during power system disturbances," *IEE Proc.-Generat., Transmiss. Distrib.*, vol. 150, no. 3, pp. 343–352, May 2003.
[12] D.-W. Xiang, S.-C. Yang, and L. Ran, "Ride-through control strategy of a doubly fed induction generator for symmetrical grid fault," *Proc. CSEE*, vol. 26, no. 3, pp. 165–170, Feb. 2006.
[13] J. Liang, D. F. Howard, J. A. Restrepo, and R. G. Harley, "Feedforward transient compensation control for DFIG wind turbines during both balanced and unbalanced grid disturbances," *IEEE Trans. Ind. Appl.*, vol. 49, no. 3, pp. 1452–1463, May/Jun. 2013.
[14] H. Nian, Y. Song, P. Zhou, and Y. He, "Improved direct power control of a wind turbine driven doubly fed induction generator during transient grid voltage unbalance," *IEEE Trans. Energy Convers.*, vol. 26, no. 3, pp. 976–986, Sep. 2011.
[15] J. Hu, J. Zhu, Y. Zhang, G. Platt, Q. Ma, and D. G. Dorrell, "Predictive direct virtual torque and power control of doubly fed induction generators for fast and smooth grid synchronization and flexible power regulation," *IEEE Trans. Power Electron.*, vol. 28, no. 7, pp. 3182–3194, Jul. 2013.
[16] V.-T. Phan and H.-H. Lee, "Improved predictive current control for unbalanced stand-alone doubly-fed induction generator-based wind power systems," *IET Electr. Power Appl.*, vol. 5, no. 3, pp. 275–287, Mar. 2011.
[17] M. I. Martinez, A. Susperregui, G. Tapia, and L. Xu, "Sliding-mode control of a wind turbine-driven double-fed induction generator under non-ideal grid voltages," *IET Renew. Power Generat.*, vol. 7, no. 4, pp. 370–379, Jul. 2013.
[18] B. Beltran, M. E. H. Benbouzid, and T. Ahmed-Ali, "High-order sliding mode control of a DFIG-based wind turbine for power maximization and grid fault tolerance," in *Proc. IEEE Int. Electr. Mach. Drives Conf.*, May 2009, pp. 183–189.
[19] Y. Yan, M. Wang, Z.-F. Song, and C.-L. Xia, "Proportional-resonant control of doubly-fed induction generator wind turbines for low-voltage ride-through enhancement," *Energies*, vol. 5, no. 11, pp. 4758–4778, Nov. 2012.
[20] J. Hu and Y.He, "Modeling and control of grid-connected voltage-sourced converters under generalized unbalanced operation conditions," *IEEE Trans. Energy Convers.*, vol. 23, no. 3, pp. 903–913, Sep. 2008.
[21] F. Morel, X. Lin-Shi, J.-M. Retif, B. Allard, and C. Buttay, "A comparative study of predictive current control schemes for a permanent-magnet synchronous machine drive," *IEEE Trans. Ind. Electron.*, vol. 56, no. 7, pp. 2715–2728, Jul. 2009.

MENG WANG received the B.E. and M.E. degrees in electrical engineering from the Anhui University of Technology, China, in 2003 and 2008, respectively, and the Ph.D. degree in electrical engineering from Tianjin University, China, in 2012. He is currently a Professor with the Department of Electronic and Electrical Engineering, Henan Normal University, China. His research interests include power electronics and the application of power electronics in renewable-energy conversion.

YANYAN SHI received the B.E. degree in automation from Qingdao University, China, in 2005, the M.E. degree in electrical engineering from the Anhui University of Technology, China, in 2008, and the Ph.D. degree in control science and engineering from Tianjin University, China, in 2012. She is currently an Associate Professor with the Department of Electronic and Electrical Engineering, Henan Normal University, China. Her research interests include wireless energy harvester and transfer.

ZHENYANG ZHANG is currently pursuing the B.E. degree with the Department of Electronic and Electrical Engineering, Henan Normal University, China. His current research interest is power electronics technology.

MINGHUI SHEN received the B.E. degrees in electrical engineering from the Henan Institute of Science and Technology, China, in 2011. He is currently an Electrical Engineer with State Grid Xinxiang Power Company, China. His research interests include development and control of high-power conversion for energy networks.

YAYING LU received the B.E. degree from Henan Normal University, China, in 2013, where she is currently pursuing the M.E. degree with the Department of Electronic and Electrical Engineering. Her current research interest is application of power electronics in renewable-energy conversion.